Voltage Sag Monitor Placement for Fault Location Detection Based on Precise Determination of Areas of Vulnerability

Mojtaba Hajiahmadi, Rahmat-Allah Hooshmand, and Arash Kiyoumarsi

***Abstract*—The increase in the number of sensitive loads in power systems has made power quality, particularly voltage sag, a prominent problem due to its effects on consumers from both the utility and customer perspectives. Thus, to evaluate the effects of voltage sag caused by short circuits, it is necessary to determine the areas of vulnerability (AOVs). In this paper, a new method is proposed for the AOV determination that is applicable to large-scale networks. The false position method (FPM) is proposed for the precise calculation of the critical points of the system lines. Furthermore, a new method is proposed for the voltage sag monitor (VSM) placement to detect the fault locations. A systematic placement scheme is used to provide the highest fault location detection (FLD) index at buses and lines for various short-circuit fault types. To assess the efficiency of the proposed methods for AOV determination and VSM placement, simulations are conducted in IEEE standard systems. The results demonstrate the accuracy of the proposed method for AOV determination. In addition, through VSM placement, the fault locations at buses and lines are detected.**

***Index Terms*—Area of vulnerability (AOV), false position method (FPM), fault location detection (FLD), power quality, voltage sag monitor (VSM).**

I. Introduction

POWER quality is one of the most critical factors that affect the reliability and operational efficiency of electric systems [1]. Among the various power quality issues, voltage sag, which directly interrupts the production processes of industrial and commercial ventures, has significant effects on consumers [2]. Moreover, complaints regarding voltage sag have surged with the increasing sensitive loads and advanced equipment such as programmable logic controllers (PLCs) and adjustable speed drives (ASDs). Therefore, it is crucial to evaluate the voltage sag based on equipment sensitivity for system customers to enhance their performance and implement effective and corrective plans [3]. IEEE Std. 1159 defines voltage sag as a reduction in root mean square (RMS) value of voltage between 0.1 and 0.9 p.u. at the power frequency for a duration of 0.5 cycles to 1 min [4]. To assess the system performance in terms of voltage sag, the vulnerability of system loads to this disturbance must be analyzed. In addition, it is essential to develop corrective schemes to improve and mitigate the voltage sag, which involves determining the areas of vulnerability (AOVs). The AOV concept describes the voltage sag propagation caused by the short-circuit fault throughout the system and its effects on the sensitive load points. For a sensitive load, the AOV encompasses the system buses and lines, and a fault that occurs in this area causes the voltage to fall below the specified threshold [5].

Various methods have been proposed to determine the AOVs. In [6], the fault voltage amplitude at the point of common coupling (PCC) is derived using a critical distance based on a voltage divider. Another method involves detecting the fault position, which relies on simulating faults at different points in a system [7], [8]. However, as power systems expand, the efficiency and accuracy of these methods decrease. To overcome the shortcomings of the previous methods, a numerical method has been introduced [5], [9]. In this method, the fault voltage equations are formulated for a sensitive load based on fault points on the system lines. The critical points (CPs) are calculated by solving these equations based on a given voltage threshold. The CPs indicate fault points on the lines, leading to a voltage magnitude at the sensitive load point equal to the given threshold. Thus, a length proportional to the total line length in the AOV is determined. The numerical method assumes that the shape of the fault voltage curve is unimodal, and the relationship between the voltage and fault points on the lines is similar to a quadratic curve. In [10], a Galerkin method is proposed to calculate the unknown coefficients by solving parametric fault voltage equations, where the fault voltage curve may have an arbitrary shape. By determining the AOV, the expected voltage sag frequency is introduced for voltage sag assessment. In [11], considering the wind turbine as a sensitive load, the allowable and non-allowable wind turbine disconnections are analyzed based on the low-voltage ride through (LVRT) requirement. In addition, the impact of photovoltaic systems on the voltage sag frequency is investigated in [12].

It is essential to determine the fault location for the nor-

Manuscript received: December 25, 2023; revised: February 23, 2024; accepted: July 26, 2024. Date of CrossCheck: July 26, 2024. Date of online publication: September 13, 2024.

M. Hajiahmadi, R.-A. Hooshmand (corresponding author), and A. Kiyoumarsi are with the Department of Electrical Engineering, Faculty of Engineering, University of Isfahan, Isfahan, Iran (e-mail: m. hajiahmadi@eng. ui. ac. ir; hooshmand_r@eng.ui.ac.ir; kiyoumarsi@eng.ui.ac.ir).

DOI: 10.35833/MPCE.2023.001022

mal operation of power system and the improvement of power quality [13]. In [14], a method is introduced based on branch current state estimation using non-synchronized measurements for the fault zone identification and fault location detection (FLD). However, because of the high cost of system monitoring, it is economically impractical to place the measurement equipment at all system buses. It is therefore essential to determine the optimal placement of voltage sag monitors (VSMs) to record voltage sag events. VSMs are identical to power quality monitors (PQMs), which are installed to measure and analyze the power quality disturbances. For the fault location, only the recorded voltage sag data are required.

Numerous studies have focused on monitor placement based on the monitor reach area (MRA) concept when considering AOVs.

With the increase in nonlinear loads and harmonic emissions in power systems, the PQM placement has been investigated by considering the AOV for voltage sag and harmonic resonance mode analysis for parallel resonance [15], [16]. In [17], the PQM placement based on the concept of symmetry is investigated to maximize the identified events in the system, which outperforms traditional voltage sag estimation and fault location techniques. The symmetry assessment is also conducted for unbalanced distribution systems in the presence of distributed generation (DG) [18]. In [19], the optimal monitor placement is proposed by considering the fault on the lines and determining the line segments based on the AOV calculated for the system buses. In [20], an optimal placement scheme of monitors is determined based on the voltage sag level in the system. Then, the state estimation model for fault location is conducted to detect the voltage sag source. In [21], an optimal PQM placement considering the graph theory is proposed to determine the voltage sag source location. In [22], the distribution system zoning is investigated based on the sag transfer coefficient, and the electrical center bus in each zone is determined as the location of VSMs. In [23], a method based on neural networks is proposed to determine the voltage sag source location and identify the sag type in the system, whereas the monitor placement is not discussed.

In this paper, a new method is proposed to determine AOVs. This method has a low computational burden and is thus particularly suitable for large networks. Accordingly, to determine the AOV for a specific bus, the evaluation commences from this bus itself. Based on the connected lines and the adjacent buses, the AOV is expanded. The AOV determination is typically conducted offline, and the real-time calculation is also feasible while considering the effects of system characteristics on the AOV. In addition, a precise method is proposed for calculating the CPs. CPs are computed for lines that are partially included in the AOV of the bus. This method ensures a high accuracy in AOV determination and guarantees convergence with fewer iterations. Furthermore, given the importance of detecting the voltage sag source locations in the system, the proposed method for VSM placement is designed to accurately detect fault locations. Thus, the VSM placement is conducted based on the AOV determination to detect fault locations at both buses and lines. Considering different short-circuit fault types in the system, we perform VSM placement separately for each fault type. As the VSM placement schemes may not be unique, the optimal one is chosen to provide the highest bus FLD and line FLD indices under all short-circuit fault types.

The main contributions of this study are as follows.

1) A false position method (FPM) is introduced for the accurate AOV determination and precise CP calculation in the system.

2) A method for VSM placement is proposed for accurate FLD based on the AOV determination and system zoning.

3) Considering the fault location on the system lines, we conduct the line segmentation and an evaluation of VSM failure scenarios to obtain the optimal placement scheme for the system.

The remainder of this paper is organized as follows. Section II introduces the fault voltage equations for the AOV determination and FLD based on the MRA matrix. Section III introduces the proposed method for AOV determination and CP calculation, and Section IV introduces the proposed method for VSM placement. Simulation results are presented in Section V, and the conclusion is given in Section VI.

II. AOV Determination and FLD

In this section, the fault voltage equations are derived based on the sequence impedance matrix to calculate the AOV for each bus in the system. The MRA matrix is established based on the effects of each bus on the others by determining the AOV of all buses. Thus, it becomes possible to distinguish the affected area of buses through the VSM placement, thereby enabling the FLD.

A. Fault Voltage Equations

First, the sequence impedance matrix of the system is obtained. As shown in Fig. 1, considering bus j as a sensitive node and utilizing the numerical method, the fault voltage equations for bus j are formed in this subsection. To calculate the AOV, the fault point K on the system lines is considered between buses F and T.

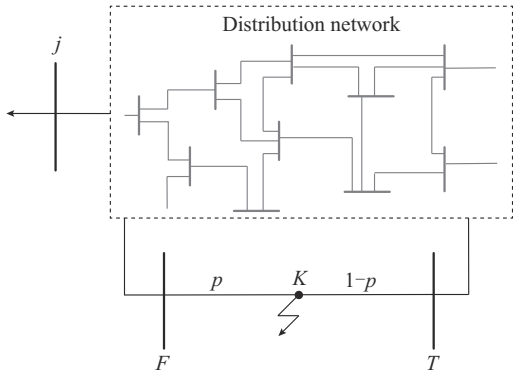

Fig. 1. Fault occurrence at point K on line F-T.

The transfer impedance between bus j and point K and

driving impedance at point K can be defined as [5]:

$$Z_{jK}^{012}=Z_{jF}^{012}+(Z_{jT}^{012}-Z_{jF}^{012})p \tag{1}$$

$$Z_{KK}^{012}=(Z_{FF}^{012}+Z_{TT}^{012}-2Z_{FT}^{012}-Z_{l}^{012})p^2+[Z_{l}^{012}-2(Z_{FF}^{012}-Z_{FT}^{012})]p+Z_{FF}^{012} \tag{2}$$

where Z_l^{012} is the sequence impedance of line l; Z_{jK}^{012} is the sequence transfer impedance between bus j and fault point K; Z_{KK}^{012} is the sequence driving impedance at fault point K; Z_{XX}^{012} is the sequence driving impedance at bus X, and X=F or T; Z_{XY}^{012} is the sequence transfer impedance between bus X and bus Y, and X, $Y=F$ or T; p is the proportion of length between bus F and fault point K to length of the entire fault line; and the superscripts 0, 1, and 2 denote the zero-, positive-, negative-sequence values, respectively.

Also, the pre-fault voltage magnitude V_K^{pref} at point K is given according to the fault position and the pre-fault voltages at buses F and T as:

$$V_K^{pref}=V_F^{pref}+(V_T^{pref}-V_F^{pref})p \tag{3}$$

Therefore, the fault voltage magnitude at bus j can be determined under different types of short-circuit faults at point K on line l. For example, when a single-line-to-ground fault (SLGF) in phase A is considered, the fault voltage at bus j for phase A $V_{A,j}^{fault}$ is given as:

$$V_{A,j}^{fault}=V_{A,j}^{pref}-\frac{Z_{jK}^{0}+Z_{jK}^{1}+Z_{jK}^{2}}{Z_{KK}^{0}+Z_{KK}^{1}+Z_{KK}^{2}}V_K^{pref} \tag{4}$$

By substituting (1)-(3) into (4), the voltage equation is derived in terms of p. The length of line segment in the AOV is then determined by solving (4), and p is thus calculated. This process is extended to all the lines in the power system to calculate the AOV. The bus vulnerability index (BVI) is obtained by considering the fault points at the buses. Subsequently, the line vulnerability index (LVI) is determined based on the BVIs of the beginning and end buses of the lines, and then the AOV is determined [5]. The fault voltage equations for other short-circuit faults such as the line-to-line fault (LLF), line-to-line-to-ground fault (LLGF), and three-phase fault (3PF) are provided in [5].

B. Establishment of Bus MRA (BMRA) and Line MRA (LMRA) Matrices

The BMRA and LMRA matrices are established by determining the AOVs for all buses based on a specified voltage threshold. In a system with N buses, the BMRA matrix has a dimension of $N\times N$, and if bus j is in the AOV of bus i, then the ij^{th} entry of BMRA matrix $BMRA_{ij}$ is equal to 1. In addition, the line segments are obtained to form the LMRA matrix by calculating the CPs of each line [19].

Figure 2(a) shows an example of the IEEE 9-bus system. Considering an SLGF and a voltage sag threshold of 0.6 p.u., the line L2 between buses 4 and 6 is used to form the LMRA matrix. In Fig. 2(b), the voltage magnitude curves for buses 1, 7, and 9 are shown considering the fault points on line L2, which is indicated by p ($p=0$ when the fault is at bus 4 and $p=1$ when the fault is at bus 6). It can be observed that line L2 has five distinct segments (s_1-s_5), and the fault in each segment causes voltage sag at specific buses. For instance, if an SLGF occurs in s_5 (p=[0.771,1]), the voltage magnitude at bus 9 falls below the threshold of 0.6 p.u., causing a voltage sag event.

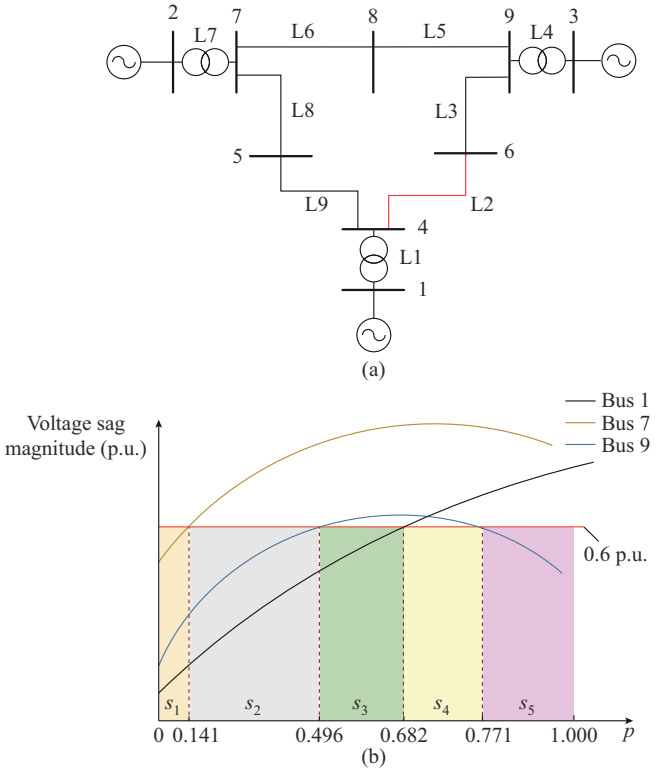

Fig. 2. Determination of line segments in an AOV. (a) IEEE 9-bus system. (b) Voltage magnitude curves at buses 1, 7, and 9.

Notably, the voltage magnitude curves of buses 2, 3, and 8 are higher than the specified threshold. Thus, a fault on line L2 does not result in a voltage sag at these three buses. In addition, the voltage magnitude curves for buses 4-6 are always below the threshold, and the entire line L2 is included in the AOV of buses 4-6. In other words, if a fault occurs on line L2, the voltages of buses 4-6 will decrease below the threshold. Consequently, the LMRA matrix for line L2 is represented by:

$$\boldsymbol{LMRA}_2=\begin{array}{c}\begin{matrix}s_1 & s_2 & s_3 & s_4 & s_5\end{matrix}\\ \begin{bmatrix}1&1&1&0&0\\0&0&0&0&0\\0&0&0&0&0\\1&1&1&1&1\\1&1&1&1&1\\1&1&1&1&1\\1&0&0&0&0\\0&0&0&0&0\\1&1&0&0&1\end{bmatrix}\end{array}\begin{array}{c}\text{Bus No.}\\1\\2\\3\\4\\5\\6\\7\\8\\9\end{array} \tag{5}$$

Taking $LMRA_{2,95}=1$ as an example, it indicates that a fault in s_5 of line L2 results in a voltage sag at bus 9. By forming the LMRA matrix for all the lines, the LMRA matrix in the system is a $9\times S$ matrix, where S represents the total number of segments across all lines.

C. Fault Location Using BMRA Matrix

Through the calculation of BMRA matrix, each bus has an AOV covered by installing a VSM at that bus. However, it cannot identify that at which bus in the AOV the fault occurs, and only the voltage sag is recorded. To determine the fault location using the BMRA matrix, the VSM placement must ensure that no identical columns exist in the fault location detection matrix (FLDM) based on the coverage area provided by each VSM. In other words, the VSM placement should result in as many distinct areas as the total number of system buses, where each bus must be located in its own separate area. In this case, it is possible to distinguish between faults occurring at different system buses.

For example, (6) presents the BMRA matrix for the SLGF in phase A in the IEEE 9-bus system. Considering the VSM locations at buses 2-4, the corresponding rows are selected from the BMRA matrix, resulting in the FLDM given in (7).

$$\boldsymbol{BMRA}=\begin{array}{c} \begin{matrix}1&2&3&4&5&6&7&8&9\end{matrix} \text{ Bus No.} \\ \begin{bmatrix}1&0&0&1&0&0&0&0&0\\0&1&0&0&0&0&1&1&0\\0&0&1&0&0&0&1&1&1\\1&0&0&1&1&1&1&0&1\\1&1&1&1&1&1&1&1&1\\1&1&1&1&1&1&1&1&1\\0&1&1&1&1&0&1&1&1\\1&1&1&1&0&0&1&1&1\\0&1&1&1&0&1&1&1&1\end{bmatrix} \begin{matrix}1\\2\\3\\4\\5\\6\\7\\8\\9\end{matrix} \end{array} \tag{6}$$

$$\boldsymbol{FLDM}=\begin{array}{c} \begin{matrix}1&2&3&4&5&6&7&8&9\end{matrix} \text{ Bus No.} \\ \begin{bmatrix}0&1&0&0&0&0&1&1&0\\0&0&1&0&0&0&1&1&1\\1&0&1&1&1&1&1&0&1\end{bmatrix} \begin{matrix}2\\3\\4\end{matrix} \end{array} \tag{7}$$

It can be observed that columns 1, 4, 5, and 6 in the FLDM are identical. Consequently, if a voltage sag is recorded by the VSM installed at bus 4, it indicates that a fault has occurred at one of these four buses. Therefore, by installing VSMs at buses 2-4, six unique columns are formed in the FLDM. Consequently, six distinct areas are obtained, and buses 1, 4, 5, and 6 are located in one of these areas. Thus, it is not possible to differentiate between faults at these buses, whereas fault locations at other buses can be recognized. For example, if the VSMs at buses 2 and 3 detect a voltage sag event and the VSM at bus 4 does not record a voltage sag, it signifies that the fault has occurred at bus 8. Therefore, to determine fault locations accurately, additional VSMs must be placed until no two identical columns are formed in the FLDM.

III. Proposed Method for AOV Determination and CP Calculation

As the number of buses and lines in a power system increases, the evaluation of all the buses and lines for AOV determination becomes more time-consuming. To address this issue, a method to simplify this process is proposed. The computational burden is significantly reduced by excluding buses and lines outside the AOV.

A. Proposed Method for AOV Determination

The AOV determination through the conventional method, relying on the BVI and LVI for large systems, is quite time-consuming. Formulating the BVI vector requires the assessment of all system buses [5]. To overcome this drawback, a new method is introduced to determine the AOV, making it feasible for implementation even in large-scale power systems.

In the proposed method for AOV determination, the assessment commences from a specific bus with a sensitive load, for which the AOV must be determined. Initially, the lines connected to the sensitive bus are evaluated using the system incidence matrix. If the end buses of these lines are in the AOV, the AOV is expanded. Figure 3 illustrates the flow chart of the proposed method for AOV determination of sensitive bus.

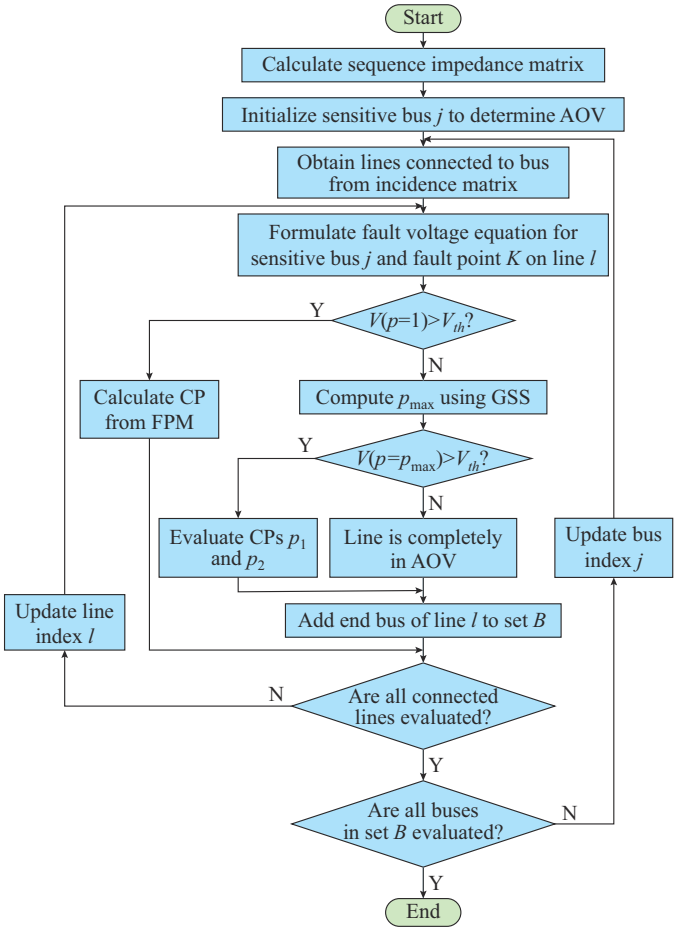

Fig. 3. Flow chart of proposed method for AOV determination of sensitive bus.

Firstly, the system sequence impedance matrix is calculated. The sensitive bus j and voltage sag threshold V_{th} is considered to determine the AOV, and the lines connected to bus j are extracted from the incidence matrix. Then, the fault voltage equation is formulated for sensitive bus j and fault point K on the line l. The voltage magnitude is then calculated at the end bus of line l by substituting $p=1$ into the fault voltage equation ($V(p=1)$).

$V(p=1)>V_{th}$ indicates that the end bus of line l is outside the AOV of bus j and line l has only one CP. The length of the line segment in the AOV of bus j is obtained by calculating the CP, and the process of AOV determination does not continue from the end bus.

$V(p=1)<V_{th}$ indicates that the end bus of line l is in the AOV of bus j. Based on the fault voltage curve, the extreme point $p_{\max}$, which indicates the fault point on the line with the highest fault voltage, is determined using the golden section search (GSS). If $V(p=p_{\max})>V_{th}$, the line is completely in the AOV; otherwise, the line has two CPs p_1 and p_2.

After the CPs of line l are computed, the end bus is added to set B, which denotes the expansion of the AOV. These steps are repeated for the buses added to set B and end until all the buses in B have been assessed. Finally, the AOV of bus j is determined. The buses and lines not evaluated previously are not in the AOV of bus j. Consequently, the sensitive bus does not experience voltage sag due to faults occurring on these lines and buses.

As an illustrative example, the proposed method for AOV determination is demonstrated for part of the hypothetical system shown in Fig. 4. Assuming bus 17 is a sensitive bus, the lines connected to this bus are identified based on the incidence matrix.

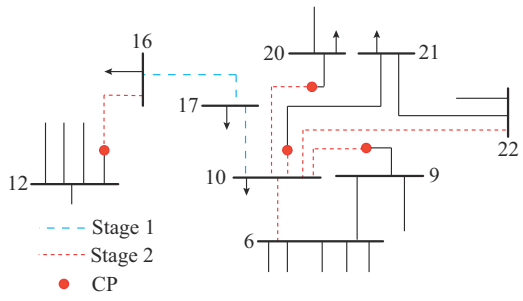

Fig. 4. Illustration of proposed method for AOV determination.

In Stage 1, the fault voltage equations for lines 17-16 and 17-10 are formulated, and the voltages at the end buses 10 and 16 are calculated. The two buses are assumed to be located in the AOV of bus 17. By computing $p_{\max}$ and assuming $V(p=p_{\max})<V_{th}$, we can conclude that these two lines are completely in the AOV of bus 17. Consequently, buses 10 and 16 are added to set B.

In Stage 2, the evaluations are performed for buses 10 and 16. Accordingly, the lines connected to buses 10 and 16 are considered, and the fault voltage equations for bus 17 are derived for the fault point on each line. For example, in the evaluation of line 16-12, the voltage magnitude at bus 17 is obtained for a fault at bus 12, and this value is assumed to exceed the defined threshold. In this case, the line has one CP, and the AOV does not expand to bus 12. For the lines connected to bus 10, the entire lines 10-22 and 10-6 are assumed to be in the AOV of bus 17. In addition, buses 9, 20, and 21 are outside the AOV, and thus the assessment does not continue for these buses. At the end of Stage 2, buses 6 and 22 are added to set B and the calculation continues for considered lines connected to these buses until the AOV for bus 17 is determined.

B. CP Calculation

In previous studies, the secant [5] and bisection [9] methods have been utilized to effectively calculate the CPs and p values in the fault voltage equations. The secant method, which is used to identify the root, depends on the determination of the initial points for computing the exact root during the iterative process. Because the order of fault voltage equations is four or higher with respect to p, the quadratic interpolation is employed to approximate the fault voltage curve and compute the initial points for the secant method. However, incorrect initial points may lead to inaccurate roots and AOV determination. In addition, in some cases, setting a small convergence tolerance or limiting the number of iterations can hinder convergence. In this regard, the bisection method [9] ensures convergence by determining roots through halving intervals that contain the root. Considering an interval $[x_l,x_u]$ for calculating the root, one drawback is that the fault voltage magnitudes at x_l and x_u, i.e., $V(x_l)$ and $V(x_u)$, respectively, are not considered when dividing the interval into equal halves. For instance, if $V(x_l)$ is closer to zero, the root is near x_l. Therefore, the bisection method requires additional iterations to extract an accurate root [24]. To overcome this shortcoming and enhance the efficiency, the FPM is proposed to obtain the CPs.

If the root exists in the interval $[x_l,x_u]$, the steps of the FPM for calculating the CPs are as follows [24].

Step 1: the lower and upper intervals are $x_l=0$ and $x_u=1$, respectively, and the voltage sag threshold V_{th} is selected.

Step 2: the fault voltage magnitudes $V(x_l)$ and $V(x_u)$ are calculated, and a value x is determined according to (8).

$$x=\frac{x_lV(x_u)-x_uV(x_l)}{V(x_u)-V(x_l)} \tag{8}$$

Step 3: if the stop criterion $\left|V(x)-V_{th}\right|<\varepsilon$ is satisfied, then x is the CP, where ε is a small positive value as the convergence tolerance; otherwise, go to *Step 4*.

Step 4: if $V(x)V(x_l)<0$, the root is in the lower sub-interval, set $x_u=x$, and return to *Step 2*; otherwise, go to *Step 5*.

Step 5: set $x_l=x$ and return to *Step 2*.

For lines with two CPs, the process involves calculating $p_{\max}$, after which *Steps 1-5* are repeated for the intervals $[0,p_{\max}]$ and $[p_{\max},1]$ to obtain the two CPs.

An additional advantage of the FPM is its independence from quadratic interpolation and approximated quadratic functions. Because p in the fault voltage equation is determined by substituting x_l and x_u, the order of fault voltage equations is inconsequential, and precise CPs are obtained using the main equation.

IV. Proposed Method for VSM Placement

After the AOV for the system buses is determined and the BMRA matrix is formed, the VSM placement is performed to detect the fault locations in the system. The proposed

method for VSM placement is presented in three steps.

A. Step 1: Solving Placement Optimization Problem

The main objective of VSM placement is to detect the fault locations in the system using the minimum number of VSMs to cover all voltage sag events. Because the VSM placement is limited to system buses, the initial VSM placement is performed based on the BMRA matrix. For a system with n buses, the objective function is defined as:

$$\min \sum_{i=1}^{n} X_i \tag{9}$$

s.t.

$$\sum_{i=1}^{n} X_i \cdot BMRA_{ij} \geq 1 \tag{10}$$

$$\sum_{i=1}^{n} X_i \left(\left| BMRA_{ij} - BMRA_{ik} \right| \right) \geq 1 \quad \forall j \neq k \tag{11}$$

where X_i is a binary variable representing the VSM placement at bus i, and $X_i = 1$ indicates that the VSM is placed at bus i.

Constraint (10) ensures that each voltage sag event is recorded by at least one VSM. In other words, each column of the FLDM must contain at least one value of 1. In addition, to distinguish between the columns in the FLDM based on the BMRA matrix discussed in Section II, (11) must be satisfied to detect the fault locations at the system buses.

The optimal location of VSMs is determined by solving the mixed-integer linear programming problem defined in (9)-(11). Two situations may arise based on the BMRA matrix. The first situation occurs when no identical columns exist in the BMRA matrix. In this case, each bus has a unique effect on the others, and the fault locations can be determined across all the buses in the system. The second situation occurs when two or more columns are identical in the BMRA matrix. This implies that these buses have the same effect, and it is not possible to distinguish the fault locations at these buses. If there are n identical columns in the BMRA matrix, it will be possible to distinguish the fault locations based on the voltage magnitude by installing $n-1$ VSMs at these buses. In this case, the bus with the lowest voltage magnitude has a fault. Consequently, the combination $C(n, n-1)$ is calculated for a set of identical columns. VSMs are then installed at the selected buses for each combination, and the placement of the remaining VSMs is determined by solving the optimization problem in (9)-(11).

For example, suppose that three columns $\{1, 5, 7\}$ in the BMRA matrix are identical. In this case, VSMs are installed at two buses in the set $\{1,5,7\}$ to detect the fault locations. Consequently, three VSM placement combinations are derived as: $\{1,5\}$, $\{1,7\}$, and $\{5,7\}$. For each combination, the variable X_i is set to be 1 for each bus i, and the optimization problem is solved.

The BMRA matrix is formed for four types of short-circuit faults: SLGF, LLF, LLGF, and 3PF. For each type of fault, the optimal VSM placement is determined by solving the optimization problem given in (9)-(11). Notably, for LLF and LLGF, where voltage sag occurs in two phases, the VSM placement scheme is obtained separately for each fault phase. For example, in the case of the LLF between phases B and C, the BMRA matrices for phases B and C are calculated, and the VSM placement scheme is derived for the voltage sag in phase B (LLF_B) and phase C (LLF_C). Similarly, for the LLGF between phases B and C, two BMRA matrices are established. Consequently, there exist six BMRA matrices corresponding to different types of short-circuit faults (SLGF, LLF_B, LLF_C, LLGF_B, LLGF_C, and 3PF), and the optimization problem is then solved for each matrix.

B. Step 2: Selecting Unique Scheme When a VSM Fails

The VSM placement schemes may not be unique for each type of short-circuit fault. In addition, because the measurement instrument may fail, it is essential to consider the effects of VSM failures on FLD. When a VSM fails, it can no longer record voltage sag events in the system. Thus, the chosen VSM placement scheme should exhibit the desired performance even in the event of a single VSM failure. Only the scenario with a single VSM failure is considered due to the low probability of simultaneous VSM failures. To determine the unique VSM placement scheme among different possible schemes for each type of short-circuit fault, the one exhibiting the highest FLD index is selected.

1) Bus FLD

Based on the BMRA matrix, the bus FLD index is calculated for each VSM placement scheme. Various VSM placement schemes are obtained for each type of short-circuit fault. Then, a single VSM failure is then considered for each placement scheme based on the number of VSMs. Thus, the bus FLD index is determined for different types of short-circuit faults in each failure scenario.

Let us define SC as a set of different types of short-circuit faults, i.e., SC={SLGF, LLF_B, LLF_C, LLGF_B, LLGF_C, 3PF}. Accordingly, for the placement scheme i related with fault type SC_k and the VSM failure at bus n, the bus FLD index for the fault type SC_j $BFLD_{SC_j}^{S_{n,i},SC_k}$ is given as:

$$BFLD_{SC_j}^{S_{n,i},SC_k} = \frac{N_b}{N_{bus}} \times 100\% \tag{12}$$

where SC_j and SC_k represent the j^{th} and k^{th} fault types in the quaternary set SC, respectively; $S_{n,i}$ represents the VSM failure scenario at bus n in the placement scheme i; N_b is the number of buses with faults detected at them; and N_{bus} is the total number of system buses.

For example, in the IEEE 9-bus system illustrated in Fig. 2(a), the LLGF between phases B and C is considered, Table I lists the bus FLD indices related to LLGF_B. Three VSM placement schemes related to LLGF_B are obtained by performing *Step 1* of the proposed method for VSM placement. For each scheme, a single VSM failure is considered, and the bus FLD index is evaluated for the SLGF, LLF, LLGF, and 3PF according to (12). For example, in scheme 1-2-3-7-8 related to the LLGF_B and the VSM failure at bus 2, the bus FLD index for LLF is calculated as $BFLD_{\text{LLF}}^{S_{2,1},\text{LLGF\_B}} = 77.78\%$. This means that if the VSM installed at bus 2 fails in scheme 1-2-3-7-8, the bus FLD index can still be up to 77.78%.

TABLE I
BUS FLD INDICES RELATED TO LLGF_B

No.	Scheme	Bus No. with VSM failure	Bus FLD index (%)				Weighted bus FLD index (%)	Sum of weighted bus FLD index (%)
			SLGF	LLF	LLGF	3PF		
1	1-2-3-7-8	1	88.89	61.11	72.22	66.67	84.17	396.67
		2	88.89	77.78	66.67	55.56	85.00	
		3	66.67	66.67	77.78	66.67	67.22	
		7	77.78	77.78	61.11	55.56	75.83	
		8	88.89	72.22	66.67	55.56	84.44	
2	1-2-3-7-9	1	88.89	72.22	77.78	66.67	85.56	427.78
		2	100.00	77.78	77.78	55.56	94.44	
		3	100.00	77.78	88.89	66.67	95.56	
		7	66.67	83.33	66.67	55.56	67.78	
		9	88.89	72.22	66.67	55.56	84.44	
3	1-2-3-8-9	1	88.89	61.11	72.22	66.67	84.17	397.78
		2	88.89	66.67	66.67	55.56	83.89	
		3	88.89	77.78	77.78	66.67	86.11	
		8	66.67	83.33	66.67	55.56	67.78	
		9	77.78	77.78	61.11	55.56	75.83	

In the bus FLD assessment, it is crucial to highlight that if m identical columns exist in the FLDM, the fault location at the buses, where the VSM is installed based on the voltage amplitude, will be detected. Considering the FLDM in (7) with $N_{bus}=9$, it is observed that columns 1, 4, 5, and 6 are identical. If the VSM is installed at bus 4, it is possible to recognize the fault location at this specific bus based on the voltage amplitude. However, the fault locations at buses 1, 5, and 6 remain undetected, resulting in $N_b=6$. The bus FLD index is then computed as: $6/9\times100\%=66.67\%$.

After the bus FLD index is calculated for all fault types in each scenario, the weighted bus FLD index is calculated considering the occurrence probabilities of SLGF, LLF, LLGF, and 3PF as 80%, 10%, 5%, and 5%, respectively. Table I lists the weighted bus FLD index in each scenario based on the occurrence probability of each fault type. Taking the failure scenario for the VSM installed at bus 2 in scheme 1-2-3-7-8 as an example, the weighted bus FLD index is $80\%\times88.89\%+10\%\times77.78\%+5\%\times66.67\%+5\%\times55.56\%=85.00\%$.

The sum of the weighted bus FLD index is then computed for each VSM placement scheme while considering the VSM failure scenario. Among the three VSM placement schemes related to LLGF_B presented in Table I, scheme 1-2-3-7-8 has the highest sum of weighted bus FLD index as 427.78%.

2) Line FLD

To extend the evaluation of FLD for faults occurring on system lines, the process is performed in a manner similar to that for buses. Accordingly, the LMRA matrix is formed based on the line segments based on the AOV for each short-circuit type. Thus, similar to (12), the line FLD index is expressed as:

$$LFLD_{SC_j}^{S_{n,i},SC_k}=\frac{N_s}{N_{SC_j}^{seg}}\times100\% \tag{13}$$

where $N_{SC_j}^{seg}$ is the total number of line segments related to the j^{th} fault type in the set SC, equivalent to the number of columns in the corresponding LMRA matrix; and N_s is the number of line segments with faults detected on them.

Thus, the line FLD index is calculated for the VSM failure at bus n and placement scheme i (scenario $S_{n,i}$) for different fault types in SC. A weighted line FLD index is then obtained for each placement scheme.

Table II lists the results of the VSM placement schemes related to LLGF_B in the IEEE 9-bus system.

TABLE II
RESULTS OF VSM PLACEMENT SCHEMES RELATED TO LLGF_B

No.	Scheme	Sum of weighted bus FLD index (%)	Sum of weighted line FLD index (%)	Total sum of weighted bus FLD and line FLD indices (%)
1	1-2-3-7-8	396.67	97.31	493.98
2	1-2-3-7-9	427.78	118.57	546.35
3	1-2-3-8-9	397.78	97.63	495.41

As indicated in Table II, the VSM placement scheme 1-2-3-7-9 achieves a total sum of the weighted bus FLD and line FLD indices of 546.35%. Thus, this scheme has a higher priority than the other two. Consequently, this scheme is chosen as the unique placement scheme related to LLGF_B.

In *Step 2*, a unique placement scheme is selected related to each fault type, resulting in a total of six unique placement schemes.

C. Step 3: Final Optimal VSM Placement of System

In *Step 3*, the bus FLD and line FLD indices are evaluated for each optimal placement scheme. The final optimal VSM placement scheme for the system is then determined based on the highest bus FLD and line FLD indices.

Figure 5 illustrates the steps of the proposed method for VSM placement in identifying fault locations at the buses and lines in the system.

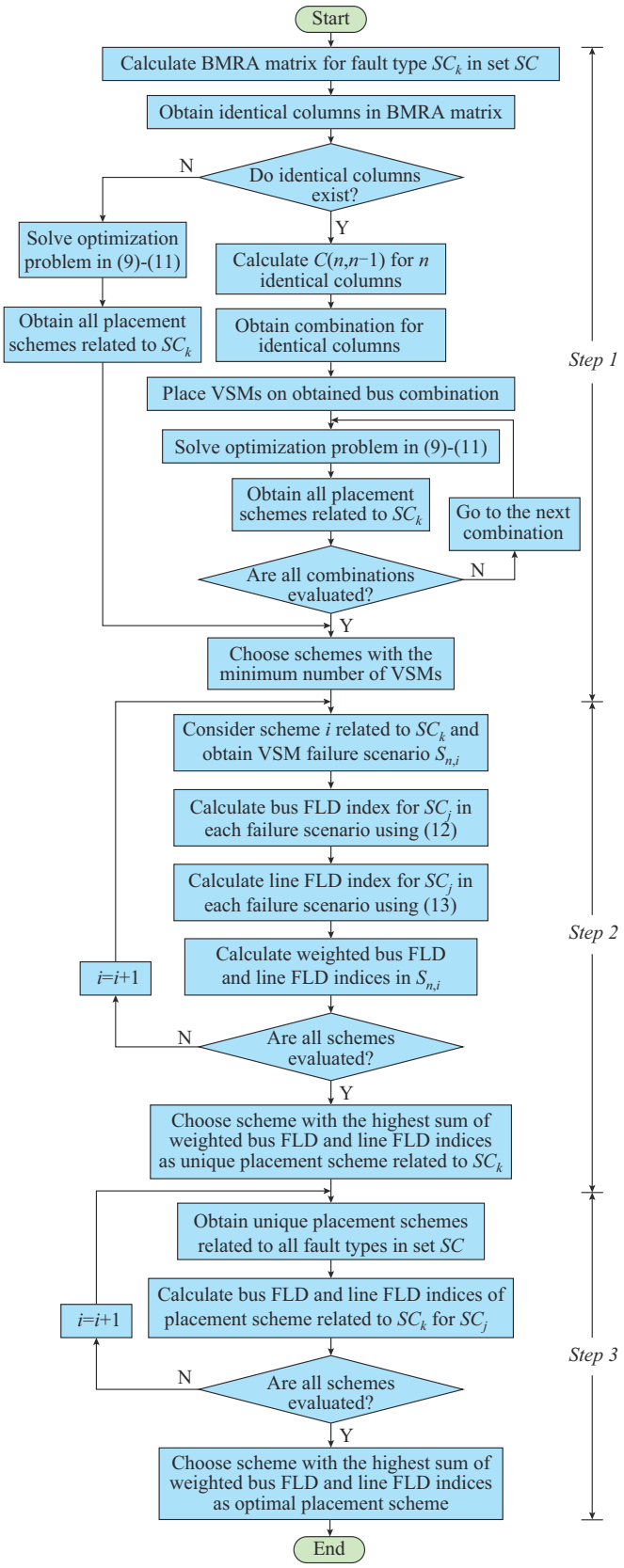

Fig. 5. Proposed method for optimal VSM placement.

V. Simulation Results

The effectiveness of the proposed methods for AOV determination and VSM placement is assessed in IEEE stardand systems. In both systems, the phase winding connection of the transformers is assumed to be Yg/Yg, and the positive-, negative-, and zero-sequence impedances of generators are specified as j0.3, j0.2, and j0.05 Ω, respectively. The zero-sequence impedances of lines are set to 2.5 times their positive-sequence impedances.

A. AOV Determination and CP Calculation

1) AOV Determination in IEEE 118-bus System

The effectiveness of the proposed method for AOV determination is assessed in the IEEE 118-bus system, which is a representation of large-scale system. The sensitive load is located at bus 70, and two assumed voltage sag thresholds of 0.7 and 0.8 p.u. are considered. Figure 6 illustrates the AOV for bus 70 under an SLGF with two voltage sag thresholds.

As shown in Table III, the proposed method and the method in [5] for AOV determination at bus 70 are compared based on the computational time.

The method in [5] requires that all system buses are evaluated to generate BVI and LVI vectors. The proposed method requires 28.86 s to determine the AOV with a voltage sag threshold of 0.7 p.u., and it significantly reduces the computational time by 32%. In addition, as the voltage sag threshold increases, resulting in the expansion of the AOV, the computational time increases. Nevertheless, the proposed method demonstrates a more efficient computation, with the AOV determined in 21.56 s, which represents a 33% reduction in computational time as compared with the method in [5].

2) Finding Precise CPs

The FPM for CP calculation is evaluated for bus 29 in the IEEE 30-bus system, and the results are compared with [5] and [9]. Considering a voltage sag threshold of 0.74 p.u. and the SLGF on line 1-3 at phase A, the fault voltage curve for bus 29 is shown in Fig. 7. Under the GSS method, the maximum value of the curve is identified at $p_{\max}=0.4084$ with a corresponding fault voltage magnitude of $V(p_{\max})=0.7437$ p. u.. Because $V(p_{\max})>0.74$ p.u., the line has two CPs. The FPM is then applied, and the CPs are obtained as $p_1=0.30365$ and $p_2=0.52028$. The different values of root p_1 obtained from the secant [5], bisection [9], and proposed methods for AOV determination are illustrated in the enlarged figure.

It is evident that the proposed method is more accurate in terms of CP calculation and has exactly detected the intersection point of the fault voltage curve and the defined voltage sag threshold. Table IV lists the comparison results for the two CPs of line 1-3 under different methods. The secant method [5] and bisection method [9] exhibit errors of 0.075% and 0.041%, respectively, whereas the proposed method has an error of only 0.001%. For long transmission lines, the secant method [5] has an error of 75 m for every 100 km of line length when determining the AOV. However, the proposed method has an error of only 1 m. Thus, the FPM method enables a more precise AOV determination.

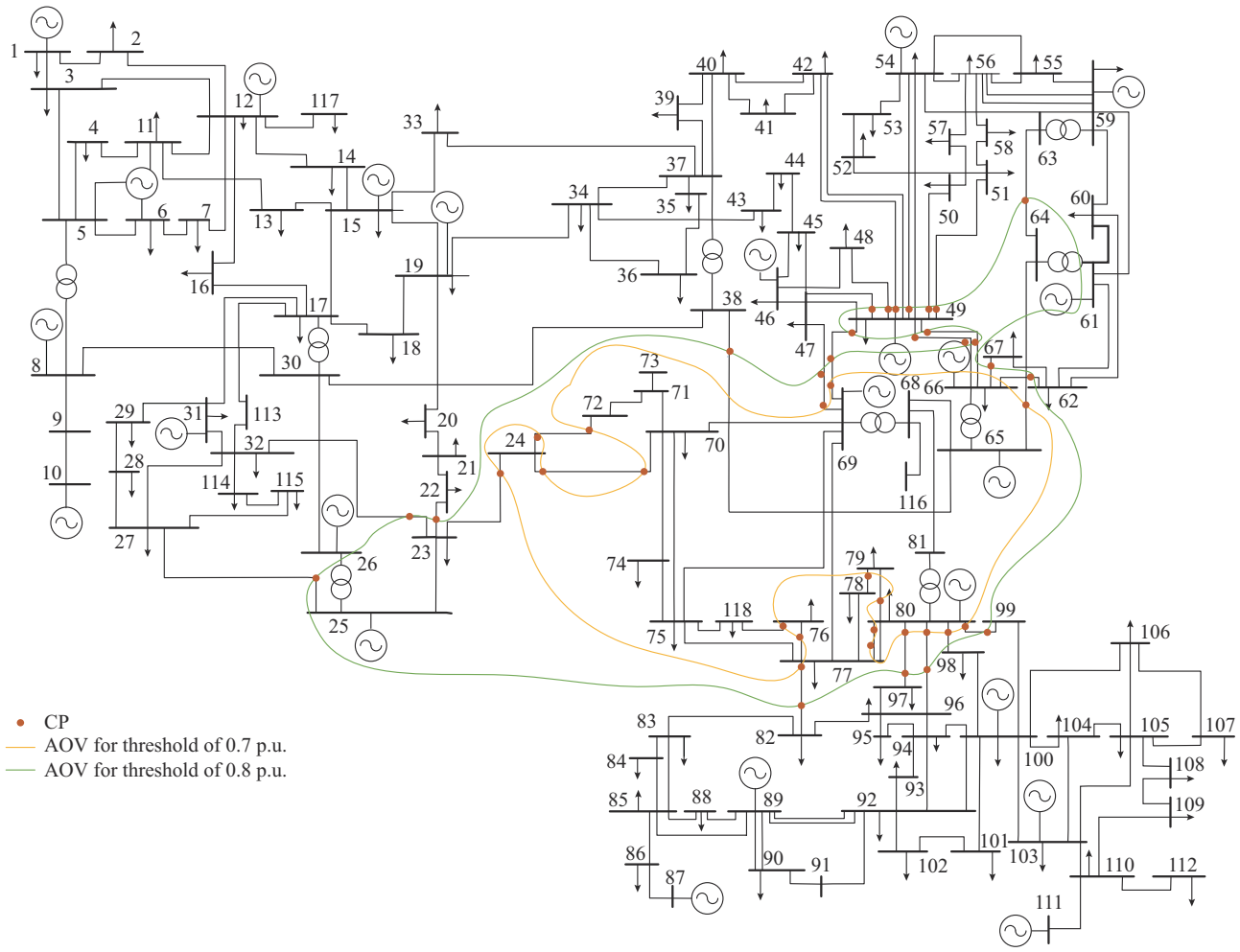

Fig. 6. AOV for bus 70 under an SLGF with voltage sag thresholds of 0.7 and 0.8 p.u..

TABLE III
COMPUTATIONAL TIME USING PROPOSED METHOD AND METHOD IN [5] FOR AOV DETERMINATION AT BUS 70

Method	Computational time (s)	
	Threshold is 0.7 p.u.	Threshold is 0.8 p.u.
[5]	28.96	31.87
Proposed	19.60	21.56

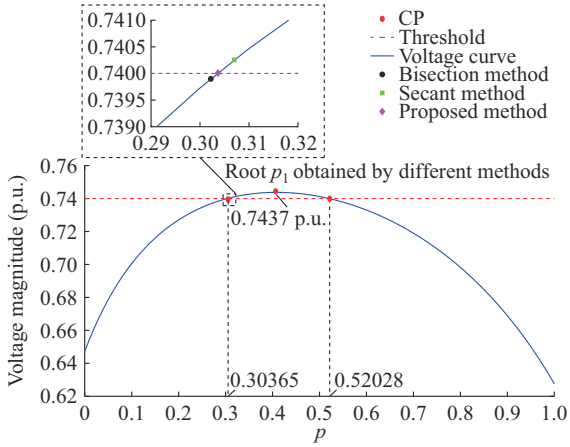

Fig. 7. Fault voltage curve of bus 29.

B. VSM Placement for FLD

The VSM placement steps are described in Section IV. The results of *Step 3* for the selection of the final optimal VSM placement scheme are evaluated. The final optimal VSM placement scheme must achieve the highest bus FLD and line FLD indices among all possible ones. Because of the effects of voltage sag on customers' equipment, it is crucial to assess the sensitivity of the equipment. Thus, the voltage tolerance curves are used to determine the voltage sag threshold, which is based on the preferences of the system operator. Because the VSM placement is proposed in the transmission system, the voltage sag threshold is set to be 0.7 p.u. while considering factors such as the fault clearance duration in the transmission system and the voltage tolerance curve.

1) VSM Placement in IEEE 9-bus System

To evaluate the proposed method for VSM placement, the implementation is carried out in the IEEE 9-bus system.

By assuming a zero-fault impedance (Z_f=0 Ω) and evaluating *Steps 1* and *2*, we obtain six unique placement schemes related to all fault types in the IEEE 9-bus system, as given in Table V. In *Step 3*, the FLD assessments are conducted for all fault types in each placement scheme considering fault locations at the buses and lines. Table V shows that the VSM placement scheme 2-3-4-7-9 achieves the weighted FLD indi-

ces of 97.22% and 38.43% for faults at buses and on lines, respectively. This placement scheme presents the highest FLD index among the schemes with the minimum number of VSMs. Although the placement scheme related to LLF_C has the highest weighted bus FLD index of 98.89%, this scheme detects only 31.47% of the fault locations on the system lines, which is a lower weighted line FLD index than that related to SLGF (38.43%). A lower weighted line FLD index indicates a higher number of line segments. For example, under the LLF_B, the system lines are divided into 25 segments. In this regard, a 9×25 LMRA matrix is determined, which is challenging to accurately distinguish fault points with a limited number of VSMs. Thus, with the chosen placement scheme with five VSMs, the fault locations in approximately 50% of these segments can be precisely detected. This does not mean that 50% of fault locations in the system remain undetected. Instead, this indicates that the fault location is identified in multiple line segments, making it challenging to specify the exact segment, where the fault has occurred. Consequently, by creating larger zones encompassing line segments with similar effects on the VSM buses, the FLD accuracy in the system can be significantly improved.

TABLE IV
COMPARISON RESULTS FOR TWO CPS OF LINE 1-3 UNDER DIFFERENT METHODS

Method	Voltage sag threshold (p.u.)	The first CP			The second CP			Total error (%)
		p_1	Voltage (p.u.)	Error (%)	p_2	Voltage (p.u.)	Error (%)	
Secant method [5]	0.74	0.30700	0.740250	0.034	0.52400	0.7397	0.041	0.075
Bisection method [9]		0.30220	0.739800	0.027	0.52118	0.7399	0.014	0.041
Proposed method		0.30365	0.740008	0.001	0.52028	0.7400	0	0.001

TABLE V
SIX UNIQUE PLACEMENT SCHEMES RELATED TO ALL FAULT TYPES IN IEEE 9-BUS SYSTEM

No.	Scheme	Fault type	Fault location	FLD index (%)						Weighted FLD index (%)	Sum of weighted FLD index (%)
				SLGF	LLF_B	LLF_C	LLGF_B	LLGF_C	3PF		
1	2-3-4-7-9	SLGF	Bus	100.00	100.00	66.67	100.00	100.00	77.78	97.22	135.65
			Line	40.00	44.00	32.26	26.67	47.37	15.38	38.43	
2	3-4-6-7-9	LLF_B	Bus	100.00	100.00	77.78	55.56	77.78	66.67	95.56	128.67
			Line	34.29	48.00	35.48	13.33	31.58	7.69	33.11	
3	1-2-5-7-9	LLF_C	Bus	100.00	100.00	100.00	100.00	100.00	77.78	98.89	130.36
			Line	31.43	40.00	29.03	26.67	42.11	23.08	31.47	
4	1-2-3-7-9	LLGF_B	Bus	100.00	100.00	77.78	100.00	100.00	66.67	97.22	129.49
			Line	31.43	44.00	25.81	46.67	52.63	23.08	32.27	
5	1-3-4-7-9	LLGF_C	Bus	100.00	100.00	77.78	77.78	100.00	66.67	96.67	134.94
			Line	40.00	44.00	29.03	26.67	47.39	15.38	38.27	
6	1-2-3-4-5-7-9	3PF	Bus	100.00	100.00	100.00	100.00	100.00	100.00	100.00	152.25
			Line	54.29	56.00	45.16	46.67	57.89	23.08	52.25	

In addition, the placement scheme 1-2-3-4-5-7-9 corresponding to the 3PF has the highest bus FLD and line FLD indices. It detects 100% of the fault locations at the system buses and 52.25% on the lines. However, this configuration requires seven VSMs, which incurs higher placement costs.

2) VSM Placement in IEEE 30-bus System

The proposed method for VSM placement is also evaluated in the IEEE 30-bus system [25], assuming a voltage sag threshold of 0.7 p.u. and considering a zero fault impedance in the system. Table VI lists the six unique placement schemes related to all fault types in the IEEE 30-bus system.

The placement scheme related to LLGF_B exhibits the highest weighted FLD index for system buses and lines. However, this placement scheme requires 16 VSMs, which incurs higher costs. The scheme with the fewest VSMs is scheme 2-6-9-11-12-19-21-24-25-29, which detects 89.58% of the fault locations at buses and 11.56% of the faults on the system lines. Notably, scheme 1-3-5-6-9-12-17-22-24-25-29 related to the SLGF, which involves 11 VSMs, enhances the sum of weighted FLD index from 101.1% to 111.7% compared with scheme 3. This reflects a 10% improvement in weighted FLD index with the addition of only one VSM.

Consequently, choosing the optimal VSM placement scheme depends on the budget constraints and FLD for the system.

3) Fault Impedance in VSM Placement

Given that faults in power systems may have impedances, simulations are conducted under different fault impedance Z_F in the IEEE 30-bus system. The increase in fault impedances leads to a smaller AOV of buses. To assess the effects of fault impedance on VSM placement, a unique placement scheme is obtained for each fault impedance under various faults types. The efficiency of each scheme is then evaluated under different fault impedances to identify the optimal placement scheme. The scheme with the highest bus FLD and line FLD indices is selected as the optimal placement scheme for the system, which demonstrates higher performance in FLD.

TABLE VI
SIX UNIQUE PLACEMENT SCHEMES RELATED TO ALL FAULT TYPES IN IEEE 30-BUS SYSTEM

No.	Scheme	Fault type	Fault location	FLD index (%)						Weighted FLD index (%)	Sum of weighted FLD index (%)
				SLGF	LLF_B	LLF_C	LLGF_B	LLGF_C	3PF		
1	1-3-5-6-9-12-17-22-24-25-29	SLGF	Bus	100.00	83.33	80.00	73.33	80.00	56.67	94.83	111.7
			Line	16.80	16.81	17.39	19.10	18.50	15.08	16.84	
2	3-5-9-14-15-17-20-22-26-27-29	LLF_B	Bus	76.67	100.00	80.00	53.33	50.00	53.33	75.58	91.7
			Line	16.02	17.95	18.01	15.97	17.32	13.07	16.10	
3	2-6-9-11-12-19-21-24-25-29	LLF_C	Bus	93.33	80.00	100.00	63.33	66.67	53.33	89.58	101.1
			Line	11.37	11.68	13.04	12.15	12.99	12.06	11.56	
4	2-5-6-8-9-11-12-13-16-19-21-22-23-24-25-29	LLGF_B	Bus	100.00	86.67	100.00	100.00	93.33	83.33	98.33	125.4
			Line	27.30	26.21	26.71	27.43	27.17	22.61	27.05	
5	1-2-3-6-7-12-13-17-19-21-23-24-26-29	LLGF_C	Bus	93.33	80.00	90.00	73.33	100.00	73.33	91.17	114.2
			Line	23.77	23.08	18.63	18.75	19.29	18.59	22.98	
6	1-2-4-6-7-9-11-12-13-16-20-21-23-26-29	3PF	Bus	93.33	83.33	93.33	73.33	73.33	100.00	92.17	115.6
			Line	24.03	22.22	18.94	20.49	20.87	22.11	23.42	

The optimal VSM placement schemes under various fault impedances in the IEEE 30-bus system are shown in Table VII. The three schemes are the unique placement schemes corresponding to the fault impedances of 0, 5, 10 Ω, respectively. Each scheme is then evaluated for other fault impedances. Table VII shows that scheme 1-4-6-7-9-12-16-17-18-22-24-27-30 achieves the highest sum of weighted bus FLD and line FLD indices. However, it requires 13 VSMs, which incurs a higher monitoring cost. By contrast, scheme 2-7-9-14-20-22-24-25-28-29 has a lower monitoring cost with a requirement of 10 VSMs, and detects fewer fault locations. According to scheme 1-3-5-6-9-12-17-22-24-25-29, the fault location accuracy is enhanced by approximately 30%, which is achieved by adding one additional VSM, compared with scheme 2-7-9-14-20-22-24-25-28-29. Consequently, scheme 1-3-5-6-9-12-17-22-24-25-29 with 11 VSMs under the fault impedance of 0 Ω is selected as the optimal placement scheme for the system. Note that for system operators who prioritize FLD over monitoring costs, scheme 1-4-6-7-9-12-16-17-18-22-24-27-30 may be preferable.

TABLE VII
OPTIMAL VSM PLACEMENT SCHEME UNDER VARIOUS FAULT IMPEDANCES IN IEEE 30-BUS SYSTEM

No.	Scheme	Z_f (Ω)	Fault location	FLD index (%)						Weighted FLD index (%)	Sum of weighted bus FLD index (%)	Sum of weighted line FLD index (%)
				SLGF	LLF_B	LLF_C	LLGF_B	LLGF_C	3PF			
1	1-3-5-6-9-12-17-22-24-25-29	0	Bus	100.00	83.33	80.00	73.33	80.00	56.67	94.83	258.83	49.43
			Line	16.80	16.81	17.39	19.10	18.50	15.08	16.84		
		5	Bus	90.00	73.33	83.33	73.33	80.00	76.67	87.50		
			Line	15.74	13.14	18.24	19.23	17.88	16.09	15.89		
		10	Bus	76.67	50.00	90.00	76.67	76.67	86.67	76.50		
			Line	16.46	17.68	16.68	17.65	17.34	17.79	16.70		
2	2-7-9-14-20-22-24-25-28-29	0	Bus	70.00	80.00	86.67	53.33	53.33	50.00	69.50	234.25	43.24
			Line	14.47	14.81	13.04	11.81	11.42	9.55	14.03		
		5	Bus	100.00	66.67	80.00	46.67	66.67	56.67	93.00		
			Line	16.05	12.04	13.21	11.89	10.93	8.81	15.11		
		10	Bus	73.33	50.00	76.67	56.67	66.67	73.33	71.75		
			Line	14.40	13.11	12.11	11.46	10.84	14.23	14.10		
3	1-4-6-7-9-12-16-17-18-22-24-27-30	0	Bus	90.00	86.67	96.67	86.67	86.67	66.67	88.83	263.5	60.11
			Line	19.64	20.23	17.39	21.53	19.69	19.10	19.58		
		5	Bus	90.00	86.67	90.00	86.67	76.67	76.67	88.75		
			Line	20.37	20.07	18.87	22.03	18.87	18.01	20.17		
		10	Bus	86.67	46.67	96.67	90.00	86.67	100.00	85.92		
			Line	20.58	18.29	18.20	20.43	17.33	22.42	20.36		

4) Comparison of Different Methods for VSM Placements in IEEE 30-bus System

A comparison is conducted between the proposed method for VSM placement and other existing methods [16], [17], [20]. As depicted in Table V, the optimal placement scheme for the IEEE 30-bus system is scheme 1-3-5-6-9-12-17-22-24-25-29. Some placement schemes obtained from other methods for the IEEE 30-bus system are listed in Table VIII. The bus FLD and line FLD indices are computed for different placement schemes under various fault types. Clearly, a higher bus FLD index is achieved under different fault types when using the proposed method for VSM placement, resulting in a higher weighted bus FLD index of 94.83%. In addition, the proposed method for VSM placement exhibits the highest weighted line FLD index, where it can accurately detect 16.84% of fault locations on the lines. Despite the higher number of VSMs in the proposed method for VSM placement, the fault location accuracy of the proposed method is more remarkable. In addition, when compared with the placement scheme in [17], which employs an equal number of VSMs as in the proposed method for VSM placement, the bus FLD and line FLD indices are approximately 7% and 3.5% higher, respectively, under the LLF_B, but they are much lower under other fault types. This reveals the effectiveness of the proposed method for VSM placement in FLD under various fault types.

TABLE VIII
COMPARISON OF DIFFERENT PLACEMENT SCHEMES IN IEEE 30-BUS SYSTEM

No.	Method	Scheme	Number of VSMs	Fault location	FLD index (%)						Weighted FLD index (%)
					SLGF	LLF_B	LLF_C	LLGF_B	LLGF_C	3PF	
1	[16]	1-3-5-7-18-24-28-30	8	Bus	43.33	46.67	33.33	43.33	40.00	26.67	42.08
				Line	8.79	10.26	7.14	9.03	7.87	6.53	8.65
2	[17]	2-4-14-15-16-19-21-22-23-25-29	11	Bus	80.00	90.00	76.67	56.67	53.33	43.33	77.25
				Line	13.12	20.23	17.70	15.97	15.35	11.55	13.75
3	[20]	2-5-6-10-17-24-26-27	8	Bus	70.00	50.00	56.67	43.33	46.67	30.00	65.08
				Line	11.11	11.96	11.49	10.76	11.42	7.54	10.99
4	Proposed	1-3-5-6-9-12-17-22-24-25-29	11	Bus	100.00	83.33	80.00	73.33	80.00	56.67	94.83
				Line	16.80	16.81	17.39	19.10	18.50	15.08	16.84

VI. CONCLUSION

This study presents a new method for determining AOVs and proposes an FPM for accurately calculating CPs, particularly for lines that are partially included in the AOV. Moreover, a VSM placement method is proposed to identify fault locations at the buses and lines in the system. These methods are implemented in the IEEE 9- and 30-bus systems. Simulation results reveal that the FPM improves the accuracy of the CP calculation as compared with other numerical methods, enabling a more precise AOV identification.

In addition, by accurately determining the AOVs and line segments based on voltage sag occurrence, the optimal location of VSMs can be determined to detect fault locations. The VSM placement scheme with the highest bus FLD and line FLD indices is selected as the optimal placement scheme for the system. The proposed method for VSM placement considers fault locations at both buses and lines to achieve a comprehensive placement scheme. Furthermore, when the placement schemes with various numbers of VSMs are obtained, the best placement plan can be chosen based on budget constraints and the FLD indices. A comparison with other placement methods demonstrates the efficiency of the proposed method in detecting fault locations.

REFERENCES

[1] A. Jalilian and S. Samadinasab, "Detection of short-term voltage disturbances and harmonics using μPMU-based variational mode extraction method," *IEEE Transactions on Instrumentation and Measurement*, vol. 70, p. 9002917, Apr. 2021.

[2] J. Y. Chan and J. V. Milanović, "Assessment of the economic value of voltage sag mitigation devices to sensitive industrial plants," *IEEE Transactions on Power Delivery*, vol. 30, no. 6, pp. 2374-2382, Dec. 2015.

[3] G. Wu, Q. Zhong, Q. He *et al*., "Evaluation method and probabilistic index of voltage sag severity considering point-on-wave," *Journal of Modern Power Systems and Clean Energy*, vol. 9, no. 3, pp. 633-638, May 2021.

[4] *IEEE Recommended Practice for Monitoring Electric Power Quality*, IEEE Std. 1159-2019, 2019.

[5] C. H. Park and G. Jang, "Systematic method to identify an area of vulnerability to voltage sags," *IEEE Transactions on Power Delivery*, vol. 32, no. 3, pp. 1583-1591, Jun. 2017.

[6] M. H. J. Bollen, "Method of critical distances for stochastic assessment of voltage sags," *IEE Proceedings: Generation, Transmission and Distribution*, vol. 145, no. 1, p. 70, Jul. 1998.

[7] G. Carpinelli, P. Caramia, C. D. Perna *et al*., "Complete matrix formulation of fault-position method for voltage-dip characterisation," *IET Generation, Transmission & Distribution*, vol. 1, no. 1, p. 56, Jan. 2007.

[8] Y. Wang, H. Luo, and X. Xiao, "Voltage sag frequency kernel density estimation method considering protection characteristics and fault distribution," *Electric Power Systems Research*, vol. 170, pp. 128-137, May 2019.

[9] S. Shakeri, S. Esmaeili, and M. H. R. Koochi, "Determining accurate area of vulnerability for reliable voltage sag assessment considering wind turbine ride-through capability," *International Journal of Electrical Power & Energy Systems*, vol. 119, p. 105875, Jul. 2020.

[10] Y. Zhou, H. Wu, B. Lou *et al.*, "Identification of the area of vulnerability to voltage sags based on Galerkin method," *Electric Power Components and Systems*, vol. 47, no. 4-5, pp. 345-356, Jul. 2019.

[11] C. H. Park and G. Jang, "Voltage quality assessment considering low voltage ride-through requirement for wind turbines," *IET Generation, Transmission & Distribution*, vol. 10, no. 16, pp. 4205-4212, Dec. 2016.

[12] N. Khatri, V. Kumar, R. C. Bansal *et al*., "Stochastic evaluation of voltage sag in power system network considering effect of photovoltaic generation," *International Transactions on Electrical Energy Sys-*

tems, vol. 29, no. 4, p. 2773, Apr. 2019.
[13] J. Hu, W. Hu, J. Chen *et al*., "Fault location and classification for distribution systems based on deep graph learning methods," *Journal of Modern Power Systems and Clean Energy*, vol. 11, no. 1, pp. 35-51, Jan. 2023.
[14] L. F. Ugarte, M. C. de Almeida, and L. H. T. Bandória, "Fault location approach to distribution networks based on custom state estimator," *Journal of Modern Power Systems and Clean Energy*, vol. 11, no. 6, pp. 1878-1889, Nov. 2023.
[15] F. B. Bottura and M. Oleskovicz, "Optimal allocation of power quality monitors considering short-duration voltage variations and parallel harmonic resonance conditions in power distribution systems," *International Journal of Electrical Power & Energy Systems*, vol. 144, p. 108580, Jan. 2023.
[16] S. Shakeri, M. H. R. Koochi, H. Ansari *et al*., "Optimal power quality monitor placement to ensure reliable monitoring of sensitive loads in the presence of voltage sags and harmonic resonances conditions," *Electric Power Systems Research*, vol. 212, p. 108623, Nov. 2022.
[17] P. E. T. Martins, W. G. Zvietcovich, T. A. de O. Silva *et al*., "Multi-objective approach for power quality monitor allocation with symmetry in short-duration voltage variations," *IEEE Transactions on Power Delivery*, vol. 34, no. 2, pp. 430-437, Apr. 2019.
[18] P. E. T. Martins and M. Oleskovicz, "Multi-objective optimization aiming to minimize the number of power quality monitors and multiple fault estimations in unbalanced power distribution systems," *IEEE Transactions on Power Delivery*, vol. 37, no. 2, pp. 1315-1323, Apr. 2022.
[19] H. Jalalat, S. Liasi, M. T. Bina *et al*., "Optimal placement of STATCOM using a reduced computational burden by minimum number of monitoring units based on area of vulnerability," *IET Generation, Transmission & Distribution*, vol. 17, no. 10, pp. 2260-2271, May 2023.
[20] G. Lv, C. Chu, Y. Zang *et al*., "Voltage sag source location estimation based on optimized configuration of monitoring points," *CPSS Transactions on Power Electronics and Applications*, vol. 6, no. 3, pp. 242-250, Sept. 2021.
[21] M. G. Tan, C. Zhang, and B. Chen, "Configuration of power quality monitor considering voltage sag location," *Electric Power Systems Research*, vol. 223, p. 109681, Oct. 2023.
[22] A. Saadat, R. A. Hooshmand, A. Kiyoumarsi *et al*., "Optimal location of voltage sag monitors in distribution networks with DGs using network zoning," *IEEE Transactions on Power Delivery*, vol. 38, no. 6, pp. 4157-4165, Dec. 2023.
[23] Y. Deng, X. Liu, R. Jia *et al*., "Sag source location and type recognition via attention-based independently recurrent neural network," *Journal of Modern Power Systems and Clean Energy*, vol. 9, no. 5, pp. 1018-1031, Sept. 2021.
[24] S. C. Chapra and R. P. Canale, *Numerical Methods for Engineers*. New York: McGraw-Hill, 2015.
[25] IEEE. (2023, Dec.). IEEE 30-bus test case. [Online]. Available: http://www.ee.washington.edu/research/pstca/pf30/pg_tca30bus.htm

Mojtaba Hajiahmadi received the B. S. degree in electrical engineering from University of Kashan, Kashan, Iran, in 2018, and the M. S. degree from University of Isfahan, Isfahan, Iran, in 2024. His research interests include power quality and power system analysis.

Rahmat-Allah Hooshmand received the B. S. degree from University of Mashhad, Mashhad, Iran, in 1989, the M.S. degree from University of Tehran, Tehran, Iran, in 1990, and the Ph.D. degree from Tarbiat Modarres University, Tehran, in 1995, all in electrical engineering. He is currently a Professor with the Electrical Engineering Department, University of Isfahan, Isfahan, Iran. His research interests include modeling of power systems and distribution networks.

Arash Kiyoumarsi received the B.S. degree in electronics engineering from Petroleum University of Technology (PUT), Ahwaz, Iran, in 1995, and the M.S. and Ph.D. degrees in electrical power engineering from Isfahan University of Technology (IUT), Isfahan, Iran, in 1998 and 2004, respectively. He is currently an Associate Professor with the Electrical Engineering Department, University of Isfahan, Isfahan, Iran. His research interests include finite element analysis in electromagnetics and electrical machines, design and analysis of interior permanent magnet synchronous machine (PMSM), and power quality analysis.